Environment Protection Engineering

Vol. 47 2021 No. 3

DOI:10.37190/epe210307

FANGLUN ZHU (ORCID 0000-0003-2745-6799)[1], CHENG ZHANG (ORCID 0000-0003-0272-9041)[1]
SHENGDAO SHAN[2] WENQIAO YUAN[3], ARTUR PAWŁOWSKI[4], CHENGFANG SONG[1]
YUCHENG CAO[1], YONGFU LI[1], JUNJIE WANGJ[1], JINYAO QIAN[1]

EFFICIENT PHOSPHATE REMOVAL IN SWINE WASTEWATEWATER USING Fe-Mn-MODIFIED PYRO/HYDROCHAR FROM SWINE MANURE

Phosphorus in wastewater is one of the main causes of water eutrophication. Phosphorus removal from swine wastewater is always a challenge. To achieve on-site recycling of swine farm waste, the low-cost pyro/hydrochars and their Fe-Mn-modified form were prepared from swine manure as an efficient adsorbent for phosphate removal. The results showed that the phosphate removal efficiency of unmodified pyro/hydrochars was less than 7.77%, which was significantly increased to 58.21–83.76% for the Fe-Mn-modified--pyro/hydrochars. The maximum adsorption capacity of pyrochar was found on the Fe-Mn-modified--pyrochar (PC-600M) with a surface area of 102.03 m^2/g and a micropore volume of 0.25 cm^3/g. The PC-600M exhibited high adsorption capacity (26.07 mg/g) in a low concentration of phosphate (50 mg/dm^3), and its removal efficiency reached up to 83.76% within 24 hours. Furthermore, the adsorption of phosphate on biochars without modification (HC-210 and PC-600) was validated using a first-order kinetic model, and the adsorption of phosphate on modified biochars (HC-210M and PC-600M) was well described by the second-order kinetic model and Langmuir isotherm. In addition, there is no significant difference in the adsorption of phosphorus between pyrochars and hydrochars, but the preparation cost of hydrochars is lower than that of pyrochars. It was confirmed that the low--cost Fe-Mn-modified pyro/hydrochar from swine manure had potential for efficient phosphate removal in wastewater treatment and would facilitate value-added utilization of swine manure.

[1]Key Laboratory of Soil Contamination Bioremediation of Zhejiang Province, Zhejiang A & F University, Hangzhou 311300, China, corresponding author Chengfang Song, email address: songcf@zafu.edu.cn

[2]Zhejiang Province Key Laboratory of Recycling and Ecological Treatment of Waste Biomass, Zhejiang University of Science and Technology, Hangzhou 310023, China.

[3]Department of Biological and Agricultural Engineering, North Carolina State University, Raleigh, NC 27695, USA.

[4]Faculty of Environmental Engineering, Lublin University of Technology, ul. Nadbystrzycka 40B, 20-618 Lublin, Poland.

1. INTRODUCTION

As necessary nutrient elements, phosphorus (P) and nitrogen (N) are essential to the primary productivity of aquatic ecosystems. However, excessive phosphate (above 0.01–0.02 mg/dm^3) and nitrogen (above 0.20–0.30 mg/dm^3) are detrimental to water quality in water bodies such as lakes and reservoirs [1]. With the rapid development of modern agricultural and industrial production, large amounts of phosphate and nitrogen effluents, especially from agricultural production and various industrial activities, are discharged into water resources, leading to water eutrophication [2, 3]. In recent years, phosphate eutrophication in water is a global problem, evident in lake quality degradation such as algal blooms, low dissolved oxygen, large-scale death of fish and other organisms, increased sediment accumulation rates, biodiversity loss, and so on [4]. In addition to causing these environmental hazards, eutrophication also increases the cost of phosphate removal and/or recycling in wastewater or sewage treatment. Therefore, there is a great need to improve the remediation of eutrophic waters and recover phosphate from wastewater.

To achieve this goal, many different technologies such as physical methods (i.e., adsorption, filtration, etc.), chemical methods (i.e., electrochemistry, precipitation, and crystallization, etc.), and biological methods, are presently used to remove phosphate from wastewater or sewage. The existing biological methods are effective in removing phosphate and have the advantage of low cost, but the process is complicated and greatly affected by the temperature and pH of the wastewater. Chemical techniques in which lime, alum, and iron salts are used have many shortcomings such as expensive chemicals, high operating costs, and secondary pollution [5]. Practical experience shows that physical treatments such as adsorption are an effective method to eliminate eutrophication of water bodies, and such treatments are widely used in various sewage treatment systems [6]. In recent years, increasing attention has been given to the development of economical and efficient phosphate removal methods without secondary pollution.

Among these technologies, the adsorption method shows promise in addressing the challenges of wastewater treatment, due to some attractive advantages such as simple process, stable disposal efficiency, low treatment cost, and fast adsorption rate, especially at low concentrations [7]. Until now, some adsorbents such as carbon materials (CMs), zeolites porous silica, and synthesized metal oxides [8], have been used for not only phosphate removal but also phosphate recovery. It is reported that CMs derived from livestock and poultry feces have good adsorption performance for both organic and inorganic pollutants [9]. In particular, swine manure is one of the most abundant worldwide, and almost half of the global production of swine manure is in China [10]. Because high volumes of swine manure can cause a series of environmental issues, many researchers have begun to study how to reduce and recycle these wastes. There has been intense interest in the fabrication of CMs from swine manure and the potential of such CMs in wastewater treatment [11].

Recently, the biochar produced from the pyrolysis of swine manure has attracted attention as an effective means for contaminant and removal of contaminants such as dyes, pesticides, and antibiotics from wastewater [9]. Moreover, swine manure itself contains water, and it can also be converted directly by hydrothermal carbonization (HTC) without drying if the manure contains 60% or more water. In terms of structure, hydrochar derived from swine manure exhibits moderate potential for the treatment of eutrophic water bodies [11]. However, the surface area of bio-/hydrochar derived from swine manure is small and shows low adsorption capacity of N, P, and other pollutants; thus, practical application of the biochar is somewhat hindered [12]. Seeking to improve the adsorption property of biochars, several researchers have reported that the biochar surface area and adsorption capacity of N and P are increased by modification of these biochars with metal (hydro) oxides, producing, for example, Mg-modified biochar, Zn--modified biochar [13], La-doped biochar, and Fe-Mn-impregnated biochar. In particular, the bimetallic modified bio-/hydrochar adsorbent is a promising alternative in wastewater treatment, owing to its high adsorption capacity and desirable catalytic performance [14]. However, there have been very few studies of Fe-Mn modified bio-/hydrochar derived from swine manure for the removal of pollutants from wastewater.

In the present study, we developed a low-cost Fe-Mn-modified pyro/hydrochar derived from swine manure for effective phosphate removal in swine wastewater. Our main objective was to compare the phosphate adsorption capacity of the pyrochar and hydrochar before and after Fe-Mn modification. The characteristics of these biochars (surface morphology, surface functional groups, etc.) were determined to understand their effects on phosphate adsorption. Furthermore, the adsorption kinetics and isotherms were investigated performed to elucidate the mechanism of phosphate adsorption by these biochars. In addition, we constructed a set of reaction beds for removing phosphate from swine farm wastewater, which has practical application value. Thus, the results of this study can provide a promising foundation for the low-cost disposal and value-added utilization of swine manure.

2. MATERIALS AND METHODS

Materials and reagents. Iron trichloride ($FeCl_3$), potassium permanganate ($KMnO_4$), and sodium nitrate ($NaNO_3$) were purchased from Sinopharm (Shanghai, China) Chemical Reagent Co., Ltd. Ammonium chloride (NH_4Cl), and sodium dihydrogen phosphate (NaH_2PO_4) were purchased from Tianjin Kemiou Chemical Reagent Co., Ltd. Sodium acetate (CH_3COONa) was purchased from Coolaber Science & Technology. All these chemicals were of analytical grade and used without further purification. The swine manure (moisture content 63.85 wt.%) was collected from a large swine farm in Hangzhou City in southeastern China.

Preparation of pyro/hydrochars. Before pyrolyzing, the excrement samples were air-dried at 105 °C and ground into the power. The treated raw materials were carbonized in a box type atmosphere furnace (AF1200-30, Shanghai Weixing Furnace Co., Ltd., China) at 400, 500, and 600 °C for one-hour retention time, with a nitrogen flow rate of 100 cm^3/min and a heating rate of 10 °C/min to obtain the pyrochar finally. For example, the material at 500 °C was denoted as PC-500. For comparison, the hydrochar from fresh swine manure was prepared using the hydrothermal liquefaction method in a 2 dm^3 stainless steel reactor (FCF-2L, Shanghai Tenheng Instrument Co., Ltd., China). The reactor was heated from room temperature to the desired temperature (180, 210, or 240 °C) for one hour at a heating rate of 5 °C/min. In a typical experiment, 500 g of fresh swine manure containing 63.85 wt. % moisture was carbonized at 210 °C to obtain the hydrochar (HC-210). All pyrochar and hydrochar samples were ground and sifted in 80 mesh sieves for the adsorption experiments.

Modification of pyro/hydrochars. The prepared biochars (pyrochars and hydrochars) were modified using Fe-Mn composites, following the method described in a previous report [13]. Briefly, 10 g of char was soaked in a 380 cm^3 solution of $FeCl_3$ and $KMnO_4$ with the Fe:Mn mass ratio 1:3, followed by mixing in an electro-thermostatic water shaker at 150 rpm for 48 h. The mixture was then centrifuged and washed with deionized water until it reached a neutral reaction. Finally, the obtained samples were dried at 105 °C for 24 h before use. The modified materials were denoted with the letter M (e.g., PC-500M or HC-210M).

Characterization of pyro/hydrochars. The pore structure characteristics of the carbon materials (CMs) were determined by means N_2 adsorption isotherms at −196 °C in a Quantachrome Autosorb iQ2 instrument, as adapted from the previous method [15]. The morphology of these samples was examined using a desktop scanning electron microscope (DSEM, Phenom ProX). Imaging was performed with a Schottky field-emission electron gun with an accelerating voltage of 5–20 kV. The FT-IR spectra of these samples were collected using a Nicolet spectrometer (iS50, Thermo Scientific) with KBr pellets in the wavelength ranges of 4000–400 cm^{-1}.

Adsorption experiments. The adsorption test was achieved by measuring the equilibrium adsorption capacity of the biochars for phosphate at room temperature. Briefly, 0.30 g of the biochar material was added to 30 cm^3 of the model phosphate solution with highly concentrated phosphate (initial phosphate concentration of 50 mg/dm^3). The mixture was kept in a thermostat shaker (150 rpm) for 12 or 24 h. The supernatant of the wastewater was then collected to measure the phosphate concentration using a multiparameter water quality analyzer (5B-6C, Yesmylab Scientific Instruments Co., Ltd., China) based on the ammonium molybdate spectrophotometric method. The effect of different biochars (HC-180, HC-210, HC-240, PC-400, PC-500, and PC-600), pH (3, 5,

7, 9, and 11), dosage of biochars (3.33, 6.67, 10.00, 13.33, and 16.67 g/dm^3), adsorption time (0–24 h), and initial phosphate concentration (50, 100, 150, 200, and 250 mg/dm^3) were investigated at room temperature. Three parallel experiments were carried out for each sample. In addition, the removal rate (%) and the biochar adsorption capacity of phosphate were calculated according to the following formulas [16]:

$$\text{Removal rate} = \frac{C_0 - C_t}{C_0} \times 100\% \tag{1}$$

$$q_t = \frac{(C_0 - C_t)V}{m} \tag{2}$$

$$q_e = \frac{(C_0 - C_e)V}{m} \tag{3}$$

where q_t and q_e are the adsorption capacities of adsorbate at time t and at equilibrium, mg/g, and C_0, C_t, and C_e represent the initial concentration, concentration at time t, and equilibrium adsorption concentration of phosphate, respectively, in the simulated wastewater, mg·dm^{-3}, V, dm^3, is the volume of the simulated wastewater, and m, g, is the weight of the pyro/hydrochars. The kinetic analysis of adsorption process was fitted using pseudo-first order, pseudo-second order, and intra-particle diffusion equations:

- pseudo-first order

$$\lg q_e - \lg(q_e - q_t) = k_1 t \tag{4}$$

- pseudo-second order

$$\frac{t}{q_t} = \frac{1}{k_2 q_e^2} + \frac{t}{q_e} \tag{5}$$

- intra-particle diffusion

$$q_t = k_{di} t^{1/2} + C_i \tag{6}$$

where q_t and q_e are the adsorption capacities of adsorbate at time t and equilibrium, mg/g, respectively. k_1, min^{-1}, and k_2, g/(mg·min), are the rate constants of the pseudo--first and pseudo-second order processes, respectively. C_i, mg/g, and k_{di}, mg/(g·min$^{1/2}$), are the constants of intra-particle diffusion model and internal diffusion rate, which is proportional to the boundary thickness.

As for the equilibrium data of phosphate sorption, the Langmuir and Freundlich isotherms were used as the analysis models for adsorption isotherms:

- Langmuir isotherm equation

$$\frac{1}{q_e} - \frac{1}{q_m K_L} \times \frac{1}{C_e} + \frac{1}{q_m} \tag{7}$$

- Freundlich isotherm equation

$$\lg q_e = \lg K_F + \frac{1}{n} \lg C_e \tag{8}$$

where q_m, mg/g, is the maximum adsorption capacity, and K_L, dm^3/mg, is the Langmuir constant, which is positively correlated with adsorption performance, and C_e, mg/dm^3, is the equilibrium concentration of the adsorbate. K_F, $mg^{1+n} \cdot dm^{-3n}/g$ is the Freundlich adsorption capacity, and n is the Freundlich constant, which represents the degree of non-linearity of the adsorption isotherm.

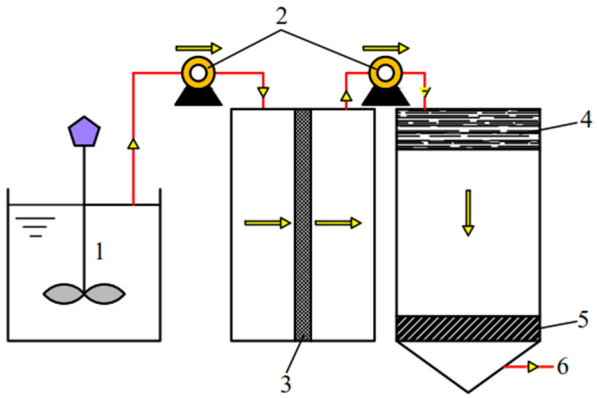

Fig. 1. Schematic diagram of experimental equipment with swine wastewater: 1 – influent tank (wastewater inlet), 2 – peristaltic pump, 3 – filter membrane, 4 – water distributor, 5 – biochar filler, 6 – treated wastewater outlet

Table 1

Some characteristic concentrations of components of wastewater after filtration membrane

pH	COD [mg O_2/dm^3]	Total phosphorus, TP [mg/dm^3]	Total nitrogen, TN [mg/dm^3]	NH_4^+-N [mg/dm^3]
6.8	3430	52.7	1140	913

Based on the above experiments, a set of pyro/hydrochar reaction beds was constructed, as shown in Fig. 1. The wastewater in the tank was pumped through the filter membrane at a speed of 50 cm^3/min by the peristaltic pump, then it was conveyed to an adsorption bed covered with 0.3 g biochar filler, finally outflowed through the water

outlet, and took the water sample every two minutes. The wastewater was taken from a biogas tank of a swine farm in Hangzhou City (which was also the source of the raw swine manure). The wastewater quality indexes after filtration membrane are shown in Table 1. There are various forms of phosphorus in actual wastewater, and phosphate is only one of them, so the TP (total phosphorus) is used to describe the results in this experiment. The TP removal rate and adsorption capacity of the reaction bed effluent were then measured using the above calculation method.

3. RESULTS AND DISCUSSION

3.1. CHARACTERIZATION OF PYRO/HYDROCHARS

The morphology and microstructures of the biochars (HC-210, PC-600, HC-210M, and PC-600M) were characterized with the use of a desktop scanning electron microscope.

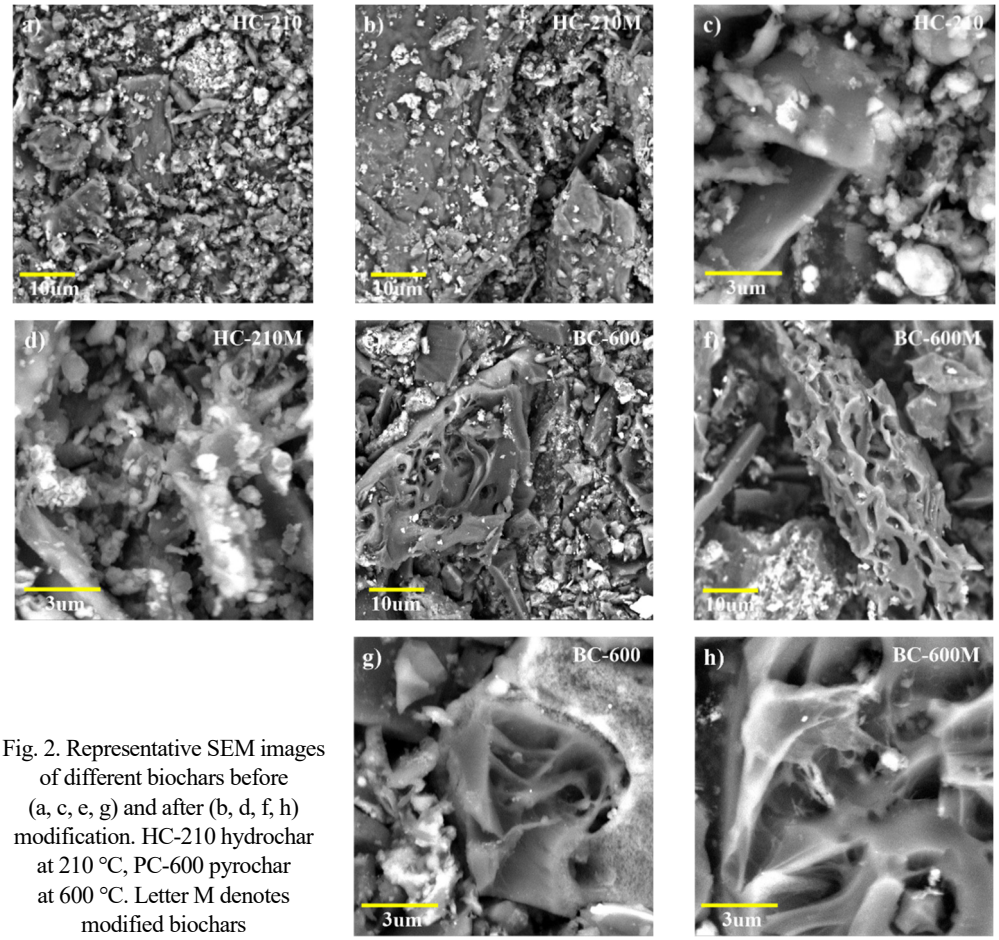

Fig. 2. Representative SEM images of different biochars before (a, c, e, g) and after (b, d, f, h) modification. HC-210 hydrochar at 210 °C, PC-600 pyrochar at 600 °C. Letter M denotes modified biochars

The images (Fig. 2) showed that the pyrochars had a larger specific surface area and richer pore structure than did the hydrochars. Compared to biochars without modification, both types of modified biochars showed numerous new pores and cracks, thereby increasing their specific surface area, which is consistent with the Brunauer–Emmett –Teller results (Table 2, and Fig. 3). Moreover, there are many fine particles on the surface of adsorbed biochars after modification, and the particle amount of modified pyrochar is more than that of modified hydrochar. It appears that the Fe-Mn modification can promote these biochars to generate large amounts of mesopores and high specific surface area, which provides more sites for phosphate adsorption [17].

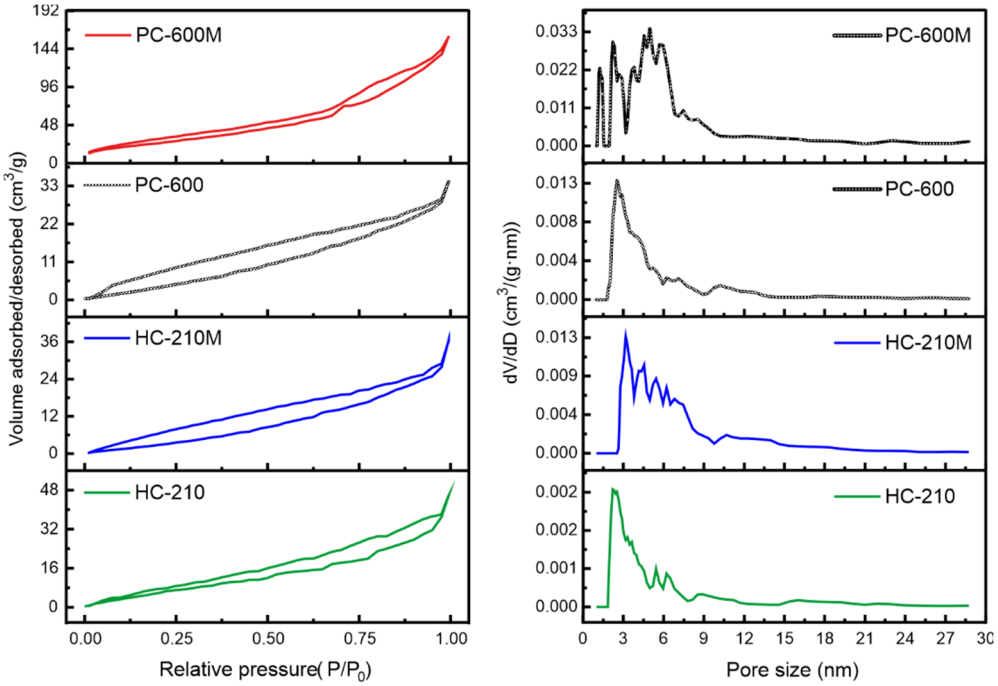

Fig. 3. Nitrogen adsorption-desorption isotherms of different biochars (left), and the pore size distributions (right) calculated from the adsorption isotherms by the density functional theory (DFT) method

We carried out measurements of N_2 adsorption-desorption at 77 K to evaluate the permanent porosity of the pyro/hydrochar samples. The N_2 adsorption-desorption isotherms are shown in Figure 3 (left). These biochars exhibited reversible type IV isotherm, which is one of the main characteristics of mesoporous materials according to the IUPAC classification [18]. In Figure 3 (right), we illustrate the pore distribution as calculated by the density functional theory (DFT) model. The results showed that the pore structure of these biochars was composed mainly of 2–10-nm mesopores, and the pore distribution was more abundant as a result of the Fe-Mn modification.

Table 2

Physical properties of different swine manure biochars

Adsorbent	S_{BET} [m^2/g]	S_{micro} [m^2/g]	S_{micro}/S_{DFT} [%]	V_{total} [cm^3/g]	D_p [nm]
HC-180	15.579	0.000	0.000	0.065	10.090
HC-210	17.081	0.802	3.809	0.071	7.636
HC-240	18.026	2.602	16.810	0.035	7.872
PC-400	26.297	0.034	0.255	0.033	4.867
PC-500	27.307	0.000	0.000	0.026	5.921
PC-600	31.334	0.089	0.483	0.053	6.780
HC-210M	25.935	0.000	0.000	0.057	7.729
PC-600M	102.028	12.046	16.386	0.248	9.726

S_{BET} – specific surface area calculated by the Brunauer–Emmett–Teller (BET) equation, S_{micro} – specific surface area of micropores calculated using the density functional theory (DFT), V_{total} – the total pore volume determined from the amount of nitrogen adsorbed at a relative pressure of 0.99, D_p – Calculated from the maximum in the Barret–Joyner–Halenda pore size distribution.

The porous textural details of these biochars are summarized in Table 2. The specific surface area of the biochars without modification increased as the temperature increased in hydrothermal and pyrolysis carbonization. The results indicate that Fe-Mn modification can effectively increase the specific surface area of biochar, especially in the case of pyrochar (PC-600M), which had a specific surface area that was more than two times higher than that of the unmodified biochar. There were no or very few micropores (only) in these biochars, which was consistent with a previous study [11]. The average size of the pores was between 4 and10 nm (consistent with the pore size distribution results, see Figure 3 right), and there was no significant change before and after modification. The total pore volume of these biochars changed slightly, except for PC-600M, which we assume was the reason for its high adsorption performance.

The functional group information characterized by Fourier transform infrared spectroscopy (FTIR) of two kinds of biochars is shown in Fig. 4. The main bands of the hydrochars include a broad absorption peak at 3330 cm^{-1}, attributed to the stretching vibration of the hydroxyl group (–OH); however, the pyrochar lacked this characteristic peak. Moreover, the bands at 2925 and 2865 cm^{-1} represent the C–H stretch of methyl and methylene, 2400–2200 cm^{-1} attributed to the stretching vibration of C≡N. Bands around 1508 cm^{-1} broadly corresponded to aromatic skeleton vibration absorption, and the band at 1600 cm^{-1} represents amino stretching [19]. These results showed that the surface functional groups of these biochars before and after modification have obvious differences in the characteristic peak of the infrared spectrum. The functional groups of the pyrochar had fewer hydroxyl, methyl, and methylene functional groups and more C–O and C–O–C groups, whereas the reverse was true for the corresponding groups of the hydrochar. Before and after modification, the stretching vibrations of C≡N in both

the hydrochar and the pyrochar were enhanced, and the characteristic peak of the aromatic carboxyl/carbonyl (C=O) of hydrochar was correspondingly enhanced, whereas the reverse is true in the case of the pyrochar. These results indicate that the Fe-Mn modification changed the strength of functional groups (such as C≡N, etc.) on the surface of these biochars, leading to the generation of more adsorption sites, which is beneficial to the adsorption of phosphate.

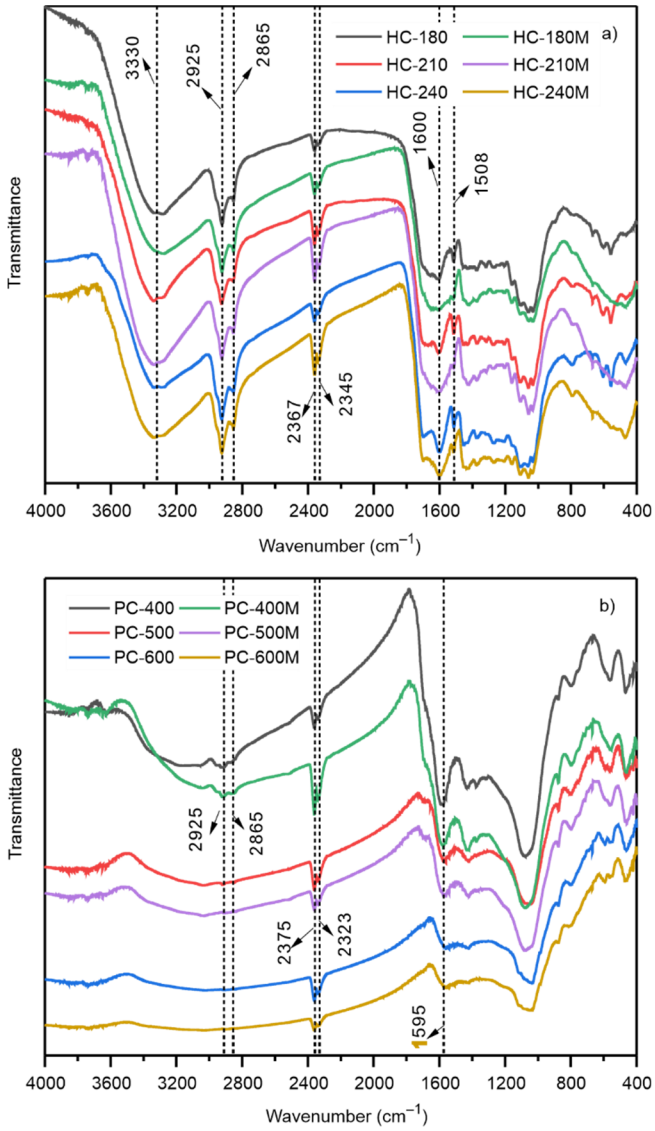

Fig. 4. FTIR images of different hydrochars (a) and pyrochars (b) before and after modification (M)

3.2. ADSORPTION CHARACTERISTICS

The changes in total phosphate content after adsorption by different biochars are shown in Fig. 5a. The adsorption effect of these two kinds of biochars without modification was weak, especially in the case of the unmodified pyrochar – in which there was almost no adsorption of phosphate.

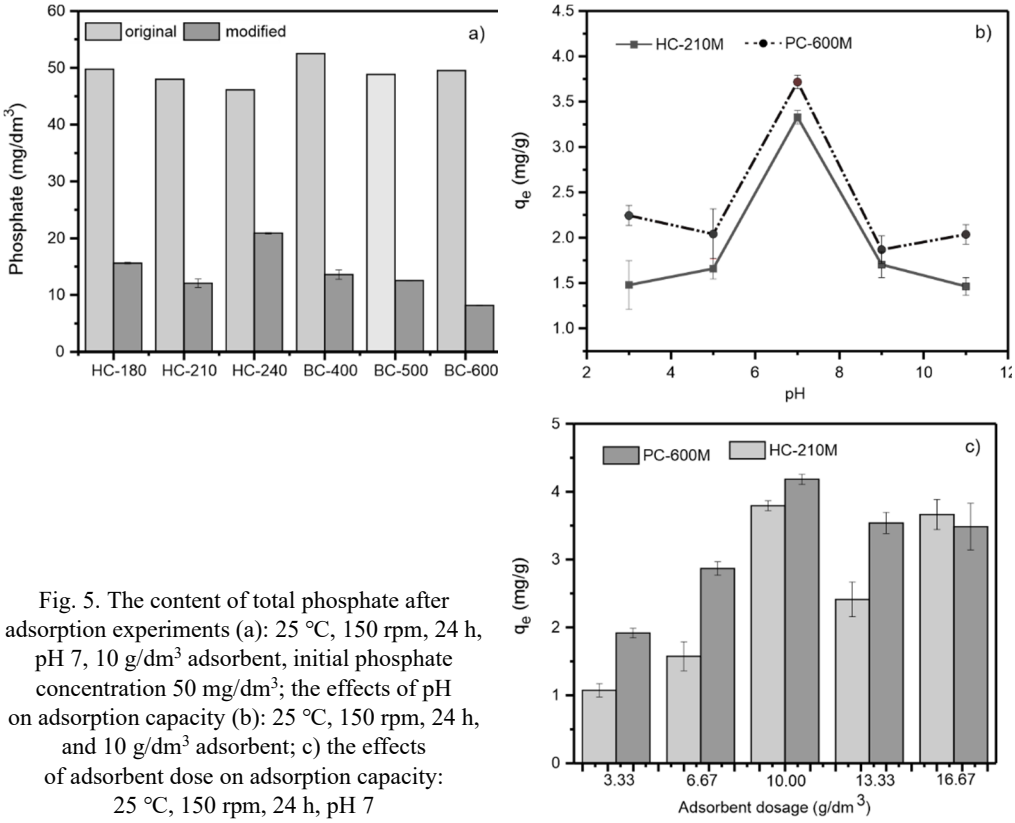

Fig. 5. The content of total phosphate after adsorption experiments (a): 25 °C, 150 rpm, 24 h, pH 7, 10 g/dm^3 adsorbent, initial phosphate concentration 50 mg/dm^3; the effects of pH on adsorption capacity (b): 25 °C, 150 rpm, 24 h, and 10 g/dm^3 adsorbent; c) the effects of adsorbent dose on adsorption capacity: 25 °C, 150 rpm, 24 h, pH 7

The reason for this phenomenon may be the presence of phosphate in pyrochar materials, and electrostatic repulsion between the negatively charged phosphate ion and the negatively charged pyrochar [3]. However, the Fe-Mn modification can significantly increase the adsorption capacity of these biochars for phosphate, and the removal rate exceeded 50%. At different preparation temperatures, the removal rate of phosphate by modified hydrochars increased first and then decreased, and the removal rate of HC-210M was as high as 76.04%. As for modified pyrochars, phosphate removal increased gradually with the increase in temperature, and the removal rate of PC-600M was as high as 83.76%. These biochars after Fe-Mn modification had Fe and Mn oxide particles attached to the surface, which caused the pH of the biochars to move toward higher values

corresponding to alkaline solution. Under neutral conditions, the positive charge on the surface of the adsorbents is increased, which enhances the electrostatic attraction to the main phosphate species, HPO_4^{2-} or $H_2PO_4^-$, and thus increases the adsorption capacity of the pyrochar for phosphate. At the same time, under the action of the Fe-Mn modification, the surface –OH functional groups of the hydrochar also increased correspondingly, which suggests the possibility of complexing with oxide functional groups to adsorb phosphate [20].

Since pH of actual swine wastewater fluctuates, we investigated the influence of HC-210M and PC-600M on the adsorption of phosphate when the pH of the model phosphate solution was between pH 3–11, as shown in Fig. 5b. With increasing the initial pH of the simulated solution, the adsorption capacities of HC-210M and PC-600M both increased initially and then decreased; the maximum adsorption capacity was reached at pH 7, (3.33 and 3.72 mg/g in HC-210M and PC-600M, respectively) and was approximately 2–3 times greater than the adsorption capacity under acidic or alkaline conditions. Because the dissociation equilibrium of phosphorus protons in an aqueous solution is greatly affected by pH, in general, phosphorus protons exist as $H_2PO_4^-$ (weak acid) and H_3PO_4 (strong acid) under acidic conditions, HPO_4^{2-} (weak base), and PO_4^{3-} (strong base) under alkaline conditions, and HPO_4^{2-} and $H_2PO_4^-$ coexisting under neutral conditions. Based on this fact, we can assume that the positively charged HC-210M and PC-600M had a strong electrostatic attraction with many negatively charged $H_2PO_4^-$ and HPO_4^{2-} under neutral conditions [21], thus greatly increasing the adsorption capacity.

The amount of adsorbent added had a significant effect on the adsorption of total phosphorus, as shown in Fig. 5c. With the increase of the dosage of these two adsorbents (from 3.33 g/dm^3 to 16.67 g/dm^3), the adsorption capacity showed a trend of initially increasing and then decreasing. When the dosage was 10 g/dm^3, the adsorption capacities of HC-210M and PC-600M both reached the maximum, at 3.79 and 4.18 mg/g, respectively. With the increase of the adsorbent dosage, the adsorption capacity of phosphate decreased slightly. This initial increase followed by a decrease was mainly due to the increase of adsorption sites on the surface of the adsorbent when the dosage is low (<10 g/dm^3), and the interaction between phosphate and the functional groups on the surface of the pyro/hydrochar was enhanced by the electrostatic and ion exchange mechanism [22]. However, under the action of high dosage (>10 g/dm^3), the accumulation of adsorbents limited the exposure of surface adsorption sites, resulting in a decrease in adsorption capacity.

3.3. ADSORPTION KINETICS

To further investigate the phosphate adsorption behavior of the experimental biochars, we designed pseudo-first order, pseudo-second order, and intra-particle diffusion models (Fig. 6). The significant factors and correlation coefficients of the kinetic model are shown in Table 3. Based on the value of R^2 obtained in the different models, the

pseudo-first order kinetics model can better explain the adsorption process of HC-210 and PC-600, whereas the pseudo-second-order kinetics model can better explain the adsorption process of HC-210M and PC-600M. The experimental data of the intra-particle diffusion model demonstrates three linear segments (Fig. 6c), indicating that the adsorption process can be described by intra particle diffusion. Moreover, the value of k_{d1} was larger than k_{d2} and k_{d3}, indicating that intraparticle diffusion was the rate-controlling process. These results indicate that the adsorption of phosphate by HC-210 and PC-600 was relatively simple and only involved the physical adsorption on the surface of biochars. However, the adsorption processes of phosphate by HC-210M and PC-600M were more complex, involving not only the simple physical adsorption on the surface of biochars but also the process of phosphate entering the pores of biochars under chemical adsorption force [22].

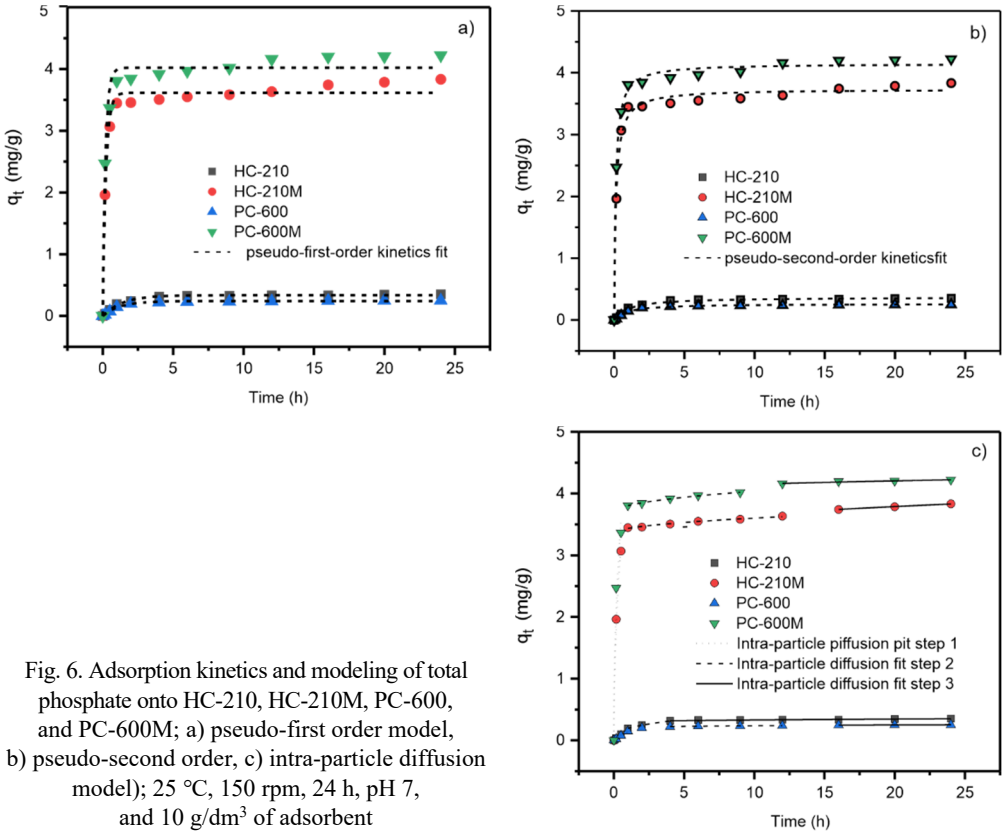

Fig. 6. Adsorption kinetics and modeling of total phosphate onto HC-210, HC-210M, PC-600, and PC-600M; a) pseudo-first order model, b) pseudo-second order, c) intra-particle diffusion model); 25 °C, 150 rpm, 24 h, pH 7, and 10 g/dm^3 of adsorbent

Generally, the adsorption mechanisms of carbon materials for phosphate mainly include ion exchange, ligand exchange, surface outer sphere complexation, surface inner sphere complexation, surface precipitation, and electrostatic attraction [23].

Table 3

Kinetic parameters for pseudo-first order, pseudo-second order, and intraparticle diffusion mechanisms of the total phosphorus onto HC-210, HC-210M, PC-600, and PC-600M

Adsorbent	Pseudo-first order			Pseudo-second order			Intraparticle diffusion								
							Step 1			Step 2			Step 3		
	q_e [mg/g]	k_1 [1/h]	R^2	q_e [mg/g]	k_2 [1/h]	R^2	C_1	k_{d1} [1/h]	R^2	C_2	k_{d2} [1/h]	R^2	C_3	k_{d3} [1/h]	R^2
HC-210	0.337 ±0.004	0.730 ±0.044	0.993	0.368 ±0.007	0.975 ±0.102	0.989	–0.006 ±0.016	0.136 ±0.034	0.940	0.075 ±0.001	0.120 ±8.069×10^{-4}	0.999	0.295 ±0.005	0.011 ±0.001	0.922
HC-210M	3.615 ±0.045	4.302 ±0.389	0.985	3.734 ±0.040	7.477 ±0.754	0.991	0.053 ±0.146	4.364 ±0.309	0.995	3.357 ±0.012	0.078 ±0.005	0.982	3.348 ±0.029	0.099 ±0.006	0.996
PC-600	0.242 ±0.003	0.835 ±0.053	0.993	0.263 ±0.006	1.098 ±0.129	0.986	–0.018 ±0.015	0.151 ±0.018	0.960	0.204 ±0.005	0.010 ±0.002	0.945	0.225 ±0.004	0.006 ±9.036×10^{-4}	0.974
PC-600M	4.019 ±0.062	4.984 ±0.583	0.976	4.148 ±0.031	8.745 ±0.658	0.995	0.147 ±0.401	4.837 ±0.850	0.970	3.695 ±0.008	0.109 ±0.004	0.996	4.021 ±0.033	0.041 ±0.008	0.931

Before modification, HC-210 and PC-600 mainly adsorbed phosphate through a small amount of active binding sites on the surface of the biochar. The large negative charge on the surface of these biochars repelled the phosphate, resulting in poor adsorption performance. After modification of these two biochars, the R^2 value of the pseudo-second order equation was higher than that of the pseudo-first order equation, indicating that chemical adsorption played a leading role. The adsorption rates and adsorption capacities of HC-210M and PC-600M were also larger in the initial stage of adsorption, which further supports this hypothesis. The adsorption capacity of PC-600M was larger than that of HC-210M, mainly because the former had a larger specific surface area than the latter. Furthermore, there were abundant pore structures on the surface, which provided more binding sites and Fe and Mn oxides.

At the same time, the precipitation of phosphate by the dissolved positively charged ions released by the adsorbent is widely considered to be the main phosphate adsorption pathway. Due to the adhesion of Fe and Mn oxides on the surface of these biochars, HC-210M and PC-600M may dissolve positively charged ions in the adsorption process, thus increasing the phosphate precipitation on the surface of the biochars. The precipitation formed by the reaction can be expressed by equations:

$$\text{Biochar}\text{——}\text{Fe}^{3+} + \text{PO}_4^{3-} \rightarrow \text{Biochar}\text{——}\text{FePO}_4 \tag{9}$$

$$\text{Biochar}\text{——}3\text{Mn}^{2+} + 2\text{PO}_3^{3-} \rightarrow \text{Biochar}\text{——}\text{Mn}_3\left(\text{PO}_4\right)_2 \tag{10}$$

The presence of Fe and Mn oxides promoted the surface complexation reaction. Under the ionic interaction between metal oxides (positively charged) and phosphate ions (negatively charged), the phosphate and the interlayer ion ($-\text{OH}^-$) exchanged to form an inner spherical surface complex [24].

3.4. ADSORPTION ISOTHERM

To further explore different possible interactions between adsorbent and adsorbate, we set up an experiment in which HC-210M and PC-600M were used to simulate the adsorption of phosphate (Fig. 7a and Table 4). Normalization was carried out according to the quality of the adsorbent, and the Langmuir model and Freundlich models were used for the simulation analysis. The results showed that when $R^2 > 0.99$, the relationship between the concentration of total phosphorus and the amount of adsorbed phosphate in the equilibrium (24 h) solution conformed to the Langmuir isotherm model.

The Langmuir isotherm adsorption model well described the adsorption of phosphate by HC-210M and PC-600M, indicating that the adsorption mechanism in these biochars was monolayer adsorption [25]. The modified biochar formed a stable molecular layer, which showed chemical adsorption to phosphate. From the R^2 values (Table 4), the Freundlich isotherm model also fitted the data well. The adsorption intensity or surface

heterogeneity (1/n) for all the biochars were less than 1, which is an indication of chemisorption process, consistent with our kinetic studies. The maximum adsorption capacity (q_m) of HC-210M and PC-600M for total phosphorus was 22.40 and 26.07 mg/g, respectively. Compared with HC-210M, PC-600M had a larger specific surface area, which provided more active adsorption sites, and had a better phosphate adsorption performance.

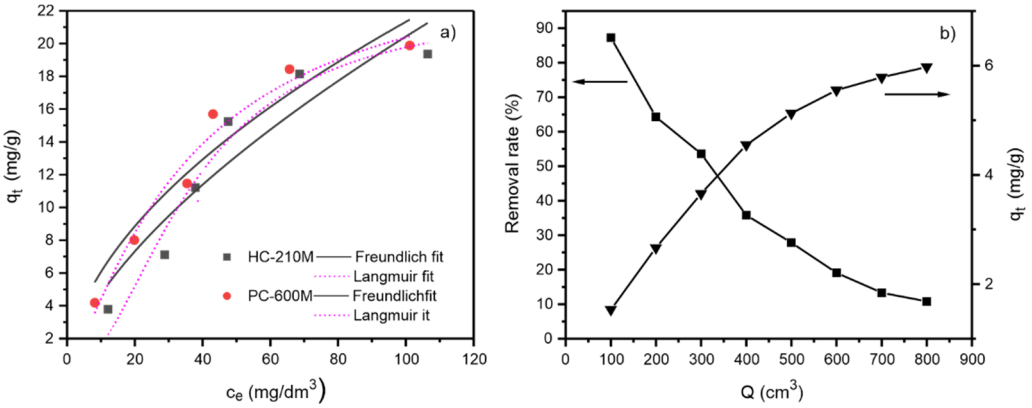

Fig. 7. Adsorption isotherms of total phosphate onto HC-210M and PC-600M (a); 25°C, 150 rpm, 24 h, pH 7, 10 g/dm^3 of adsorbent; TP removal rate and cumulative adsorption capacity of the system with PC-600M (b); 25°C, pH 7, and 0.3 g of adsorbent

Table 4

Adsorption isotherm parameters of total phosphate onto HC-210M and PC-600M

Adsorbent	Langmuir isotherm			Freundlich isotherm		
	q_m [mg/g]	K_L [dm^3/mg]	R^2	1/n	K_F [mg^{1+n}·dm^{-3n}/g]	R^2
HC-210M	22.396±3.574	7.571E-4±0.002	0.938	0.638±0.133	1.082±0.608	0.863
PC-600M	26.069±6.016	0.011±0.010	0.957	0.547±0.088	1.720±0.621	0.919

3.5. PRACTICAL APPLICATION IN SWINE WASTEWATER

Based on these experimental results, we concluded that PC-600M had a higher pore volume rate and specific surface area, resulting in a better phosphate removal effect. For this reason, we constructed a set of reaction beds for removing phosphorus from swine farm wastewater. The removal effect is shown in Fig. 7b. With the amount of wastewater passed through the bed increased, the removal rate of total phosphorus by the reaction bed gradually decreased, and the adsorption capacity gradually reached the saturation value of 5.97 mg/g. We found that the removal rate of total phosphorus in the effluent was the highest (87.24%) when the amount of wastewater passed through the bed was 100 cm^3. Therefore, the system has a strong potential to remove total phosphorus in swine farm wastewater.

4. CONCLUSIONS

The Fe-Mn modified biochars derived from swine manure have good phosphate adsorption performance, having been shown to increase the removal rate of phosphate in wastewater by more than 70.0% compared to the biochars without modification. In particular, the HC-210M and PC-600M biochars had the highest phosphate removal rates, 73.02%, and 83.76%, respectively. Characterization of these biochars showed that Fe-Mn modification can significantly improve the surface structure and physicochemical properties, thereby increasing the adsorption efficiency of phosphate. Moreover, the adsorption of phosphate on the initial biochars (HC-210 and PC-600) was validated by the first-order kinetic model, whereas the adsorption of phosphate on modified biochars (HC-210M and PC-600M) was well described by the second-order kinetic model. The adsorption isotherms of HC-210M and PC-600M were consistent with the Langmuir isotherm adsorption model, and the maximum adsorption capacities were 22.40 and 26.07 mg/g, respectively. The adsorption of phosphate on the modified biochars was highly dependent on pH. With the initial simulated solution changing from acidic to basic, the adsorption capacities of HC-210M and PC-600M both increased initially and then decreased. In the neutral environment (pH 7), the maximum adsorption capacity is reached, at a level that is more than 90% higher than the minimum adsorption capacity under acidic or alkaline conditions. With the results of this study, we can confirm that low-cost Fe-Mn-modified pyro/hydrochar from swine manure has the potential for efficient phosphate removal in wastewater treatment. By carbonizing and modifying swine manure to create an adsorbent for phosphate we can "use waste to treat waste", thus providing a low-cost and effective method for sewage treatment in swine farms.

ACKNOWLEDGEMENTS

This work was supported by the Zhejiang Province Key Research and Development Plan (2020C01017), National Natural Science Foundation of China (41501341), Zhejiang Province Natural Science Foundation (LY16D010011), and the Scientific Research Foundation of Zhejiang A & F University (2034020096). We thank the reviewers for their positive and constructive comments.

REFERENCES

[1] PARK J., WANG J.J., XIAO R., ZHOU B., DELAUNE R.D., SEO D., *Effect of pyrolysis temperature on phosphate adsorption characteristics and mechanisms of crawfish char*, J. Coll. Interf. Sci., 2018, 525, 143–151. DOI: 10.1016/j.jcis.2018.04.078.

[2] JIAO G.J., MA J., LI Y., JIN D., GUO Y., ZHOU J., SUN R., *Enhanced adsorption activity for phosphate removal by functional lignin-derived carbon-based adsorbent: Optimization, performance and evaluation*, Sci. Total Environ., 2020, 761, 143217. DOI: 10.1016/j.scitotenv.2020.143217.

[3] BACELO H., PINTOR A.M.A., SANTOS S.C.R., BOAVENTURA R.A.R., BOTELHO C.M.S., *Performance and prospects of different adsorbents for phosphorus uptake and recovery from water*, Chem. Eng. J., 2020, 381, 122566. DOI: 10.1016/j.cej.2019.122566.

[4] LI X., KUANG Y., CHEN J., WU D., *Competitive adsorption of phosphate and dissolved organic carbon on lanthanum modified zeolite*, J. Coll. Interf. Sci., 2020, 574, 197–206. DOI: 10.1016/j.jcis. 2020.04.050.
[5] CHEN F.F., LI H.F., JIA X.R., WANG Z.Y., LIANG X., QIN Y.Y., CHEN W.Q., AO T.Q., *Characteristic and model of phosphate adsorption by activated carbon electrodes in capacitive deionization*, Sep. Purif. Technol. 2020, 236, 116285. DOI: 10.1016/j.seppur.2019.116285.
[6] HUANG W., ZHANG Y., LI D., *Adsorptive removal of phosphate from water using mesoporous materials. A review*, J. Environ. Manage., 2017, 193, 470–482. DOI: 10.1016/j.jenvman.2017.02.030.
[7] KARTHIKEYAN P., MEENAKSHI S., *Synthesis and characterization of Zn-Al LDHs/activated carbon composite and its adsorption properties for phosphate and nitrate ions in aqueous medium*, J. Mol. Liq., 2019, 296, 111766. DOI: 10.1016/j.molliq.2019.111766.
[8] WEI T., LI Q., WANG H.J., ZHANG G., ZHANG T., LONG Z., XIAN G., *Advanced phosphate and nitrogen removal in water by La-Mg composite*, Environ. Res., 2021, 193, 110529. DOI: 10.1016/j.envres. 2020.110529.
[9] FENG L., LI X., CHEN X., HUANG Y., PENG K., HUANG Y., YAN Y., CHEN Y., *Pig manure-derived nitrogen-doped mesoporous carbon for adsorption and catalytic oxidation of tetracycline*, Sci. Total Environ., 2020, 708, 135071. DOI: 10.1016/j.scitotenv.2019.135071.
[10] LARSON C., *China's lakes of pig manure spawn antibiotic resistance*, Science, 2015, 80 (347), 704–704. DOI: 10.1126/science.347.6223.704.
[11] LIU Y., YAO S., WANG Y., LU H., BRAR S.K., YANG S., *Bio- and hydrochars from rice straw and pig manure. Inter-comparison*, Bioresour. Technol., 2017, 235, 332–337. DOI: 10.1016/j.biortech. 2017.03.103.
[12] ZHANG P., SUN H., YU L., SUN T., *Adsorption and catalytic hydrolysis of carbaryl and atrazine on pig manure-derived biochars. Impact of structural properties of biochars*, J. Hazard. Mater., 2013, 244–245, 217–224. DOI: 10.1016/j.jhazmat.2012.11.046.
[13] CHEN L., JIANG X., XIE R., ZHANG Y., JIN Y., JIANG W., *A novel porous biochar-supported Fe-Mn composite as a persulfate activator for the removal of Acid Red 88*, Sep. Purif. Technol., 2020, 250, 117232. DOI: 10.1016/j.seppur.2020.117232.
[14] YAN L., LIU Y., ZHANG Y., LIU S., WANG C., CHEN W., LIU C., CHEN Z., ZHANG Y., *$ZnCl_2$ modified biochar derived from aerobic granular sludge for developed microporosity and enhanced adsorption to tetracycline*, Bioresour. Technol., 2020, 297, 122381. DOI: 10.1016/j.biortech.2019.122381.
[15] ZHANG C., JIA C., CAO Y., YAO Y., XIE S., ZHANG S., LIN H., *Water-assisted selective hydrodeoxygenation of phenol to benzene over the Ru composite catalyst in the biphasic process*, Green Chem., 2019, 21, 1668–1679. DOI: 10.1039/c8gc04017f.
[16] TANG M., JIA R., KAN H., LIU Z., YANG S., SUN L., YANG Y., *Kinetic, isotherm, and thermodynamic studies of the adsorption of dye from aqueous solution by propylene glycol adipate-modified cellulose aerogel*, Coll. Surf. A, Physicochem. Eng. Asp., 2020, 602, 125009. DOI: 10.1016/j.colsurfa. 2020.125009.
[17] LI J., LI B., HUANG H., LV X., ZHAO N., GUO G., ZHANG D., *Removal of phosphate from aqueous solution by dolomite-modified biochar derived from urban dewatered sewage sludge*, Sci. Total Environ., 2019, 687, 460–469. DOI: 10.1016/j.scitotenv.2019.05.400.
[18] MUTTAKIN M., MITRA S., THU K., ITO K., SAHA B.B., *Theoretical framework to evaluate minimum desorption temperature for IUPAC classified adsorption isotherms*, Int. J. Heat Mass Transf., 2018, 122, 795–805. DOI: 10.1016/j.ijheatmasstransfer.2018.01.107.
[19] HOU Y., HUANG G., LI J., YANG Q., HUANG S., CAI J., *Hydrothermal conversion of bamboo shoot shell to biochar: Preliminary studies of adsorption equilibrium and kinetics for rhodamine B removal*, J. Anal. Appl. Pyrol., 2019, 143, 104694. DOI: 10.1016/j.jaap.2019.104694.
[20] TRAZZI P.A., LEAHY J.J., HAYES M.H.B., KWAPINSKI W., *Adsorption and desorption of phosphate on biochars*, J. Environ. Chem. Eng., 2016, 4, 37–46. DOI:10.1016/j.jece.2015.11.005.

[21] ALAGHA O., MANZAR M.S., ZUBAIR M., ANIL I., MU'AZU N.D., QURESHI A., *Comparative adsorptive removal of phosphate and nitrate from wastewater using biochar-MgAl LDH nanocomposites. Coexisting anions effect and mechanistic studies*, Nanomat., 2020, 10 (2), 336. DOI: 10.3390/nano 10020336.

[22] ZHU Z., HUANG C.P., ZHU Y., WEI W., QIN H., *A hierarchical porous adsorbent of nano-α-Fe_2O_3/Fe_3O_4 on bamboo biochar (HPA-Fe/C-B) for the removal of phosphate from water*, J. Water Proc. Eng., 2018, 25, 96–104. DOI: 10.1016/j.jwpe.2018.05.010.

[23] ZHANG M., GAO B., *Removal of arsenic, methylene blue, and phosphate by biochar/AlOOH nanocomposite*, Chem. Eng. J., 2013, 226, 286–292. DOI: 10.1016/j.cej.2013.04.077.

[24] VIKRANT K., KIM K.H., OK Y.S., TSANG D.C.W., TSANG Y.F., GIRI B.S., SINGH R.S., *Engineered/designer biochar for the removal of phosphate in water and wastewater*, Sci. Total Environ., 2018, 616–617, 1242–1260. DOI: 10.1016/j.scitotenv.2017.10.193.

[25] GU L., DONG G., YU H., ZHANG K., LU X., WEN H., ZOU T., *Preparation of porous biochar by urine assisted pyrolysis of sewage sludge and their application for Eriochrome Black T adsorption*, J. Anal. Appl. Pyrol., 2020, 153, 104975. DOI: 10.1016/j.jaap.2020.104975.